Constraints on the depth and variability of the lunar regolith

B. B. WILCOX[1], M. S. ROBINSON[2], P. C. THOMAS[3], and B. R. HAWKE[1]

[1]Hawai'i Institute of Geophysics and Planetology, University of Hawai'i, 2525 Correa Road, Honolulu, Hawai'i 96822, USA
[2]Center for Planetary Sciences, Northwestern University, 1850 Campus Drive, Evanston, Illinois 60208, USA
[3]Center for Radiophysics and Space Research, Cornell University, Ithaca, New York 14850, USA
[*]Corresponding author. E-mail: bbwilcox@higp.hawaii.edu

Abstract–Knowledge of regolith depth structure is important for a variety of studies of the Moon and other bodies such as Mercury and asteroids. Lunar regolith depths have been estimated using morphological techniques (i.e., Quaide and Oberbeck 1968; Shoemaker and Morris 1969), crater counting techniques (Shoemaker et al. 1969), and seismic studies (i.e., Watkins and Kovach 1973; Cooper et al. 1974). These diverse methods provide good first order estimates of regolith depths across large distances (tens to hundreds of kilometers), but may not clearly elucidate the variability of regolith depth locally (100 m to km scale). In order to better constrain the regional average depth and local variability of the regolith, we investigate several techniques. First, we find that the apparent equilibrium diameter of a crater population increases with an increasing solar incidence angle, and this affects the inferred regolith depth by increasing the range of predicted depths (from ~7–15 m depth at 100 m equilibrium diameter to ~8–40 m at 300 m equilibrium diameter). Second, we examine the frequency and distribution of blocky craters in selected lunar mare areas and find a range of regolith depths (8–31 m) that compares favorably with results from the equilibrium diameter method (8–33 m) for areas of similar age (~2.5 billion years). Finally, we examine the utility of using Clementine optical maturity parameter images (Lucey et al. 2000) to determine regolith depth. The resolution of Clementine images (100 m/pixel) prohibits determination of absolute depths, but this method has the potential to give relative depths, and if higher resolution spectral data were available could yield absolute depths.

INTRODUCTION

Regolith covers virtually the entire lunar surface and thus provides a substantial amount of our information about the Moon. The regolith has been imaged, sieved, raked, cored, walked on, driven across, modeled, studied, and pondered, yet its complexities continue to cloak details of its depth and structure. Studies dating back to the earliest days of lunar exploration have attempted to determine the depth of the regolith remotely by using small crater morphology (e.g., Quaide and Oberbeck 1968), the blockiness of craters over a range of sizes (Shoemaker and Morris 1969), and the number of craters per unit area (Shoemaker et al. 1969). However, there are important discrepancies among these morphological indicators, which should draw attention to the variability of the regolith thickness and help elucidate the three-dimensional nature of the regolith. Therefore, we have conducted a detailed study of crater size-frequency populations and the frequency and distribution of blocky craters in selected lunar regions in order to investigate thickness variations in the mare regolith. Finally, we investigate the utility of using optical maturity maps to infer regolith depths and show this method to be promising, but currently of limited utility due to a lack of 10 m scale multispectral imaging.

BACKGROUND

There has been significant debate as to what actually constitutes the lunar regolith. Merrill (1897) first defined the term "regolith" for terrestrial applications. He stated, "In places this covering is made up of material originating through rock-weathering or plant growth in situ. In other instances it is of fragmental and more or less decomposed matter drifted by wind, water or ice from other sources. This entire mantle of unconsolidated material, whatever its nature or origin, it is proposed to call the regolith." When adapted to the Moon on the basis of observations at the Surveyor III site,
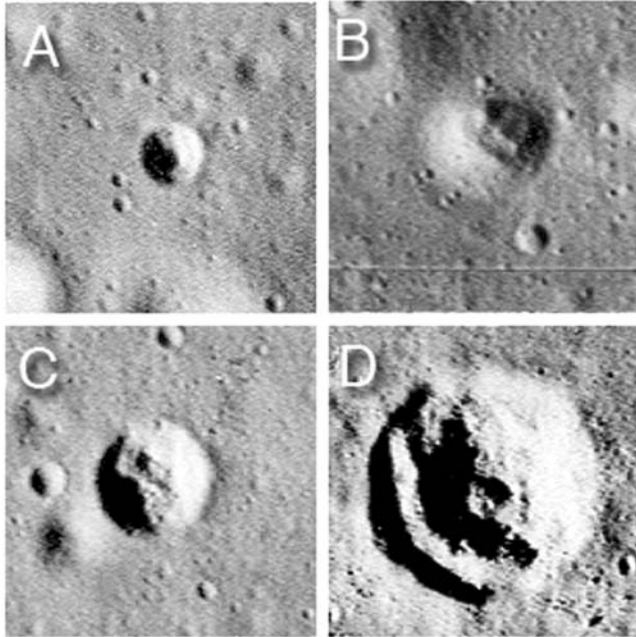
Fig. 1. Four classes of small craters as defined by Quaide and Oberbeck (1968). a) Normal, bowl-shaped morphology; b) central mound; c) flat-bottomed; d) concentric. Crater morphology is dependent on depth to a strength interface; craters trend A–D with decreasing depth of surficial layer. Each scene is 119 m across, from LO3-188-H2.

the regolith was defined in a similar matter: as a layer of fragmental debris of relatively low cohesion overlying a more coherent substratum (Shoemaker et al. 1967). Subsequently, in regards to the Surveyor VII site situated on the ejecta of the Tycho crater, Shoemaker et al. (1968) refined their definition of the regolith to exclude "widespread blankets of fragmental ejecta associated with large, individual craters." Instead, the definition of regolith was restricted to include only the "thin layer of material that forms and progressively evolves over a longer period of time as a result of an extremely large number of individual events." This definition sought to provide a distinction between the upper heavily reworked zone and the lower zone of debris of large-basin-forming or crater-forming events. Oberbeck et al. (1973) took exception to this definition because the "regolith is not completely reworked but is frequently stratified with interlayers of reworked fine-grained material and little modified coarser-grained debris. An upper reworked zone cannot be rigorously defined in the classic localities, nor is an unambiguous division possible in those cases where ejecta breccias have been cratered and modified subsequent to their deposition." They proposed that a definition more similar to the original terrestrial definition be adopted. They argued that the "classic mare regolith is not just the reworked surface layer but is the entire blanket of rock debris overlying cohesive substrate rocks." In the highlands the picture is even more complicated, as noted by Cintala and McBride (1995), where the surfaces are "so pulverized from

accumulated impacts that they have no bedrock layer for reference" and "the local definition of regolith becomes more philosophical in nature." Here we adopt the looser definition of Merrill (1897) as applied to the Moon by Oberbeck et al. (1973), and include all fragmental debris overlying largely coherent rock as regolith. However, we note that for most localities, there probably does not exist a clearly identifiable contact between fractured material above and coherent material below. As Merrill (1897) explained, the regolith can be either "found lying on a rocky floor of little changed material, or becomes less and less decomposed from the surface downward until it passes by imperceptible gradations into solid rock."

Traditionally, the main method of estimating lunar regolith depth has been through the study of small crater (<250 m) morphology, which was shown by Quaide and Oberbeck (1968) to be dependent on the nature and depth of the substrate. From Lunar Orbiter (LO) images, they recognized four classes of small craters: normal bowl-shaped, central mound, flat-bottomed, and concentric or bench (Fig. 1). To understand the underlying causes of these morphologies, they impacted various target materials with a projectile from a high-velocity gun and thus showed that strength boundaries control crater interior morphology. Quaide and Oberbeck used a simple "fines-on-solid" model of 24-mesh quartz sand over a flat, more coherent substrate to represent regolith on top of basalt. For the substrate material, they used 24-mesh quartz sand bonded by epoxy resin to unconfined compressive strengths of ~1.4 and ~68.5 bar. With both of these substrate strengths, they were able to create each of the observed small crater morphologies by varying the thickness of the unconsolidated surficial layer. They showed that normal craters form when the unconsolidated surficial material has a relative thickness greater than some value between $D_A/3.8$ and $D_A/4.2$, where D_A is the apparent crater diameter. Similarly, concentric craters form only when the regolith has a thickness less than some value between $D_A/8$ and $D_A/10$. Quaide and Oberbeck (1968) and Oberbeck and Quaide (1968) used these relationships to estimate the depth of the surficial layer (regolith) on mare deposits from orbital photography, finding depths ranging from 1–6 m to 1–16 m in their various mare study areas.

In their calculations, it was assumed that the interface responsible for producing the various crater morphologies was the mare basalt bedrock surface. However, this interface is not necessarily bedrock and, strictly speaking, should only be described as an interface between materials with contrasting physical properties. While the 68.5 bar material used in their experiments can represent coherent bedrock, the 1.4 bar material is so weak that it could easily be crushed by hand, and thus does not represent physical properties of coherent bedrock. That this weaker material, when serving as "coherent substrate," still produced the same morphologies, suggests that any simple strength discontinuity could be the

underlying cause of different crater morphologies in some of the observed craters. In their experiments, even a thin layer of paint between two layers of sand was sufficient to produce a crater with irregular walls (Oberbeck, personal communication).

Evidence that weak strength discontinuities (as compared to bedrock) can cause bench morphology came when Apollo astronauts visited several bench craters (Bench crater at the Apollo 12 site, the Station 9 crater at the Apollo 15 site, Plum crater at the Apollo 16 site, and Van Serg crater at the Apollo 17 site). It was found that none of these craters formed in bedrock and that the benches were due to impacts in targets with units of differing physical properties, such as a resistant layer within the regolith (Shoemaker et al. 1970; Muehlberger et al. 1972, 1973; Swann et al. 1972; Schmitt 1973).

Another possible indicator that a portion of the bench craters may be due to factors other than bedrock is the existence of relatively fresh bench craters without large block populations (Fig. 2). Bench craters that penetrated through the regolith and partially formed in bedrock would excavate part of that bedrock, thus forming blocks. As discussed below, the lack of blocks is another indicator that the bench morphology may not always be due to bedrock. Thus, it is misleading to assume that bench morphology represents a regolith/rock interface in all cases.

Another common method for estimating regolith thickness is based on the occurrence (or lack thereof) of blocks produced during an impact event. Rennilson et al. (1966) suggested that the depth of the fragmental layer (regolith) could be estimated from the depth of the smallest crater with a blocky rim. This logic assumes that craters with blocks penetrated through the regolith to a more coherent or coarser-grained substrate that fractures into blocks; craters without blocks form solely in unconsolidated regolith. Using blocks as indicators of regolith thickness assumes that in general, small differences in age (and thus degradation state) of craters alone cannot account for the presence or absence of blocks because blocks on the lunar surface erode slowly. Erosion caused by impacts that are small compared to the size of the rock ("single particle abrasion") is at a rate on the order of 1 mm/10^6 years (Crozaz et al. 1971; Gault et al. 1972; Hörz et al. 1974). "Catastrophic rupture," caused by impacts resulting in a crater, the diameter of which is at least a quarter of the diameter of the rock, is a more effective process in removing blocks. However, these impact events occur less frequently and the median survival time for a boulder approximately 3 m across (a size typical in this study) is still on the order of 10^9 years (Hörz 1977). Though blocks can escape destruction for substantial periods of time, they are likely to spend part of their lifetime buried within the regolith (Hörz 1977). Thus, the most degraded craters cannot be used for estimating regolith depth because of the likelihood of their block populations being buried.
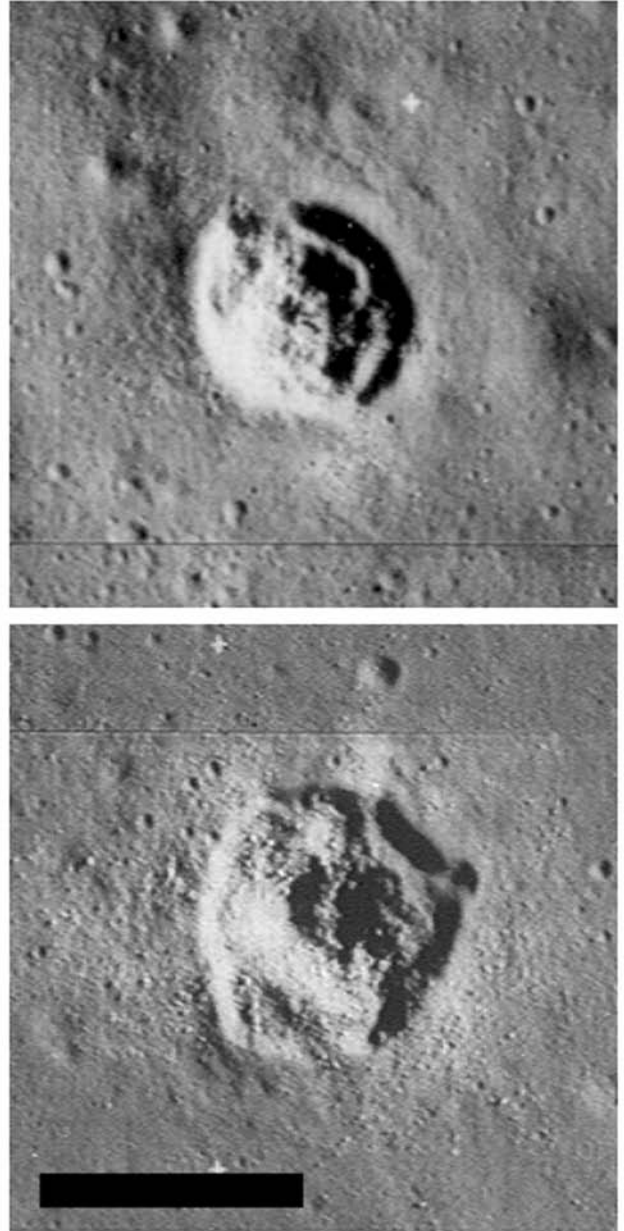

Fig. 2. Bench craters with differing block populations. The top crater (LO3-188-H2) has very few blocks, while the bottom crater (LO3-196-H2) has abundant blocks, indicating that it has excavated more coherent material than the top crater. Scale bar is 100 m.

Relatively shallow regolith depths of between 2–15 cm and 8–10 m were estimated in the vicinity of Surveyor landers by mapping blocky craters (Shoemaker and Morris 1969). However, the irregular spatial distribution of blocky craters has not been fully considered. Craters similar in diameter, and degradation state can be found in close proximity, one with no blocks, the other with many (Fig. 3). These apparently inconsistent blocky crater pairings cannot be readily explained by a simple, shallow regolith model, and the
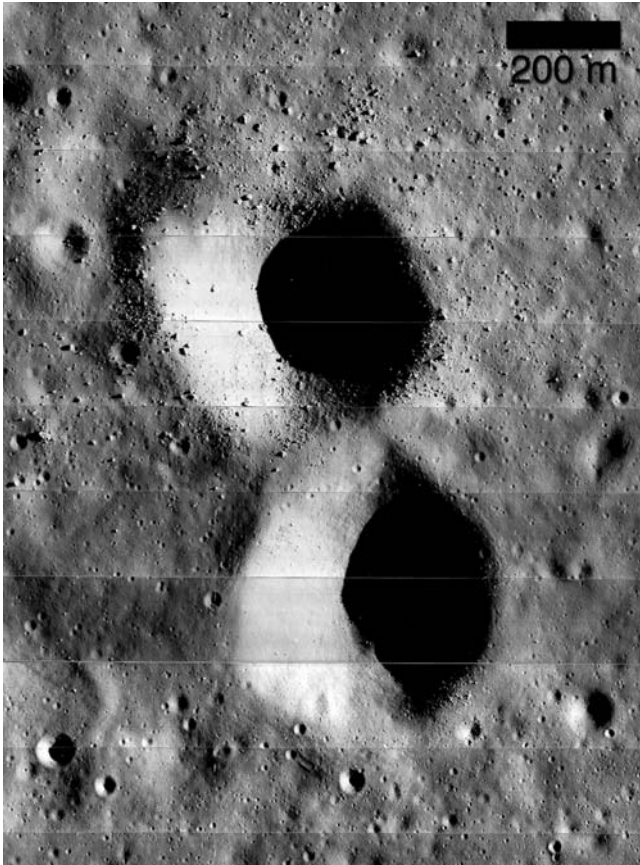
Fig. 3. An example of craters of similar size and morphology, with different block populations. The top crater (595 m in diameter) has abundant blocks; the bottom crater (575 m in diameter) has no detectable blocks, possibly indicating heterogeneities in regolith depth. From LO2-161-H2.

implications for the variability of regolith depth have not been thoroughly examined.

Another possible complication with the blocky crater method of determining regolith depth is the existence of regolith breccia boulders. In several cases, astronauts observed craters (e.g., Van Serg at the Apollo 17 site) that appeared to have excavated large amounts of coherent substrate producing a significant population of blocks, but upon inspection, the blocks turned out to be extremely friable regolith breccias (Muehlberger et al. 1973; Schmitt 1973). In these cases, the blocks produced by a crater-forming event are not excavated from the coherent substrate, but rather are formed from induration of regolith, probably during the impact event that deposited them on the surface (Muehlberger et al. 1973; Schmitt 1973). From existing orbital photography, it is not possible to discriminate between these two types of blocks; regolith depth estimated from these impact-produced rocks would be shallower than the actual depth. There is also the possibility that blocks around a crater were excavated from a blocky layer in the regolith, or from large, isolated, buried blocks. In this case, too, the regolith depth inferred

from this type of crater would be shallower than the actual depth. The depths estimated from this method are thus likely to err on the shallow side.

Because regolith on the Moon is produced by impacts, the thickness of the regolith should correlate directly with crater abundance, and thus regolith depth has also been estimated by examining the size-frequency distribution of crater populations (Shoemaker et al. 1969). As a crater population matures, the number of craters that are visible on the surface is less than the number of craters that were actually produced because new craters obliterate older ones. The diameter at which the cumulative number of craters seen on the surface is less than the number produced is the equilibrium diameter; this diameter can be identified as a break in slope in a cumulative histogram of crater size-frequency (Gault 1970; Schultz et al. 1977). Below the break in slope (larger diameters), the trend is representative of the production population of craters; above the break in slope (smaller diameters), the trend represents the steady-state craters of which more were produced than are still visible on the surface. For the steady-state craters, the difference between the production population of craters and the population of craters still visible on the surface represents the number of craters that were destroyed. This population of obliterated craters initially starts as voids in the surface, but as they age, their uplifted rims erode and their interiors fill with regolith until they become shallow to the point that they are no longer distinguishable (Shoemaker et al. 1969; Soderblom 1970). The depth of the regolith in a local area is thus equal to the initial depth of the destroyed craters minus the rim height (Shoemaker et al. 1969). Over large areas, the average regolith depth must be proportional to the depth of the equilibrium crater population. Thus, accurate determination of the diameter at which a crater population has reached equilibrium is a powerful tool for estimating regolith depth in a given area.

The incidence angle (deviation of sun vector from surface normal) affects the number of craters that can be readily identified in an image; fewer craters are visible in images with lower incidence angles (angles closer to solar zenith). This effect is more important for degraded craters, the walls of which have shallower slopes. The incidence angle of an image may affect the identification of degraded craters, resulting in uncertainties in estimates of the equilibrium diameter of a population.

Regolith depth has also been examined seismically. At the Apollo 12, 14, and 15 sites, some information about the three-dimensional nature of the regolith was gleaned incidentally from passive seismic experiments designed to study deeper features (Latham et al. 1970, 1971, 1972). At the Apollo 14, 16, and 17 sites, active seismic experiments were designed to provide data to specifically characterize the regolith and regolith depth estimates were obtained from seismic refraction profiling. Apollos 14 and 16 landed in non-
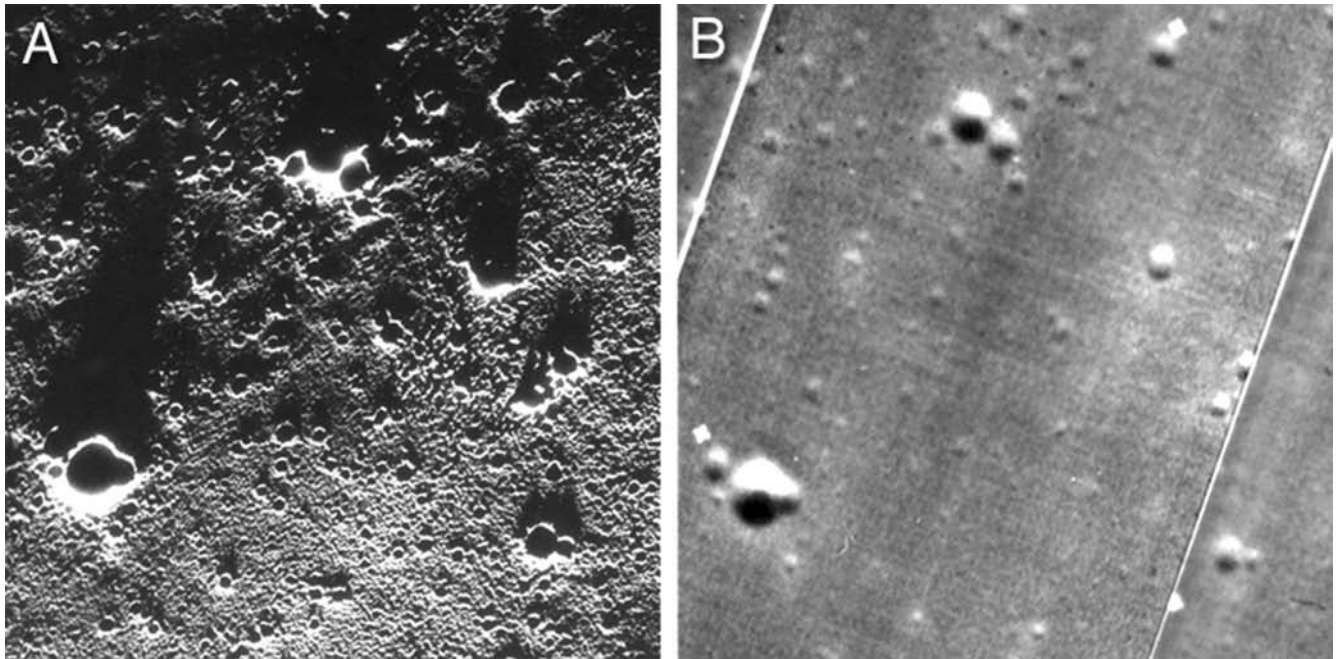
Fig. 4. The same area under different lighting conditions, after Soderblom (1972). Scene is ~16.4 km across. a) Our 89° incidence angle study area (AS15-98-13347). b) A 70° incidence angle LO image (LO4-163-H1). Many more craters are visible in the high incidence angle image. The low resolution of the LO image (>40 m/pixel) did not allow direct quantitative comparison of crater populations.

mare areas, and the sites were estimated to have regolith depths of 8.5 m and 12.2 m, respectively (Watkins and Kovach 1973). At the Apollo 17 mare site, several distinct layers were identified. In a regional seismic profile model, the first 4 m of the surface were interpreted to be regolith; below that, a layer interpreted to be rubble of older regolith, extremely fractured rock, or both, extended from 4 m down to 32 m. Below 32 m was a layer interpreted to be fractured or vesicular basalt (Cooper et al. 1974). An alternate regional model includes only a 7–12 m layer of regolith atop a fractured or vesicular basalt (Cooper et al. 1974). These numbers should be viewed with caution; the results depend on a number of assumptions and can differ markedly (as in the two examples above) when parameters or assumptions are varied. For example, it was reported that relief of up to 6 m in subsurface layers could be observed in the seismic data, but in the regional seismic model, it is assumed that all layers are planar and their physical properties are uniform, resulting in an oversimplified representation of the regolith depth (Cooper et al. 1974). Also, the seismic data are not internally consistent: the regional profile that incorporates all seismic source data does not agree with an end-to-end profile, which uses only select seismic sources, where there is an additional layer at a depth of 65 m (Cooper et al. 1974).

While these techniques (crater morphology, block population, equilibrium diameter, and seismic) provide useful tools for estimating regolith depth, many issues remain open. Why aren't all fresh bench craters blocky? If there are many large (>100 m), buried craters, why are such small thicknesses (1–10 m) generally cited? Why aren't all large,

fresh craters blocky? How important is the variation in regolith thickness? Shortcomings in previous estimates may be due to a regolith that is more complex (not a simple two-layer model, with regolith atop a planar bedrock layer) and/or a regolith with significantly variable depth in a local area. The work presented in this paper is designed to further examine regolith depth and local spatial heterogeneities in regolith depth.

METHODS AND RESULTS

Equilibrium Diameters

We have employed the equilibrium diameter method to determine regolith depth and investigated the effects of solar incidence angle on the equilibrium diameter of crater size-frequency distributions of mare areas of similar ages. Because higher incidence angles enhance more subtle topographic features, the sun angle should have a direct effect on the number of craters visible in an image, with more craters detectable at higher incidence angles (Soderblom 1972; Young 1975). This in turn should have a direct effect on the regolith depth estimated using the crater size-frequency method of Shoemaker et al. (1969). In order to investigate sun angle effects, we compared the apparent crater populations and equilibrium diameters of images with incidence angles of 71°, 79°, and 89°. Each image was converted to digital format by scanning the image at the highest resolution necessary to preserve all of the information inherent in the original photograph.
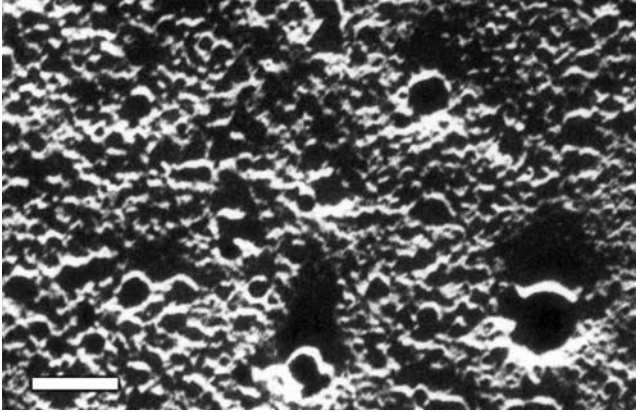
Fig. 5. A portion of our 89° incidence angle study area (Fig. 4a, AS15-98-13347) showing the nearly "shoulder-to-shoulder" distribution of 100–300 m craters (Soderblom 1972). Scale bar is 1 km.

Our first study site is a 950 km² area located in Oceanus Procellarum (approximately 26°N, 58°W), ~275 km from the 40-km crater Aristarchus. For this location, there exists extremely high incidence angle data; in fact, the terminator crosses the image AS15-98-13347. The effective resolution of this photograph is ~9 m/pixel, similar to the typical LO medium resolution images (~7 m/pixel), and is sufficient for the size range of craters we are investigating (>25 m) (Fig. 4). Soderblom (1972) observed that in the near-terminator image, craters 100–300 m in diameter are so ubiquitous that they are positioned "shoulder-to-shoulder" (Fig. 5). While this observation has been widely cited, no crater count data from this high incidence angle image was reported. This site has an estimated age of 2.76 billion years (+0.30, −0.18) (Hiesinger et al. 2003), as determined by comparing the regional crater size-frequency distribution to the lunar crater production function established from radiometric ages of returned samples.

The second and third sites are also in Oceanus Procellarum. Site number two is a 173 km² area covered by the 79° incidence angle image LO3-165-M (~1.7°N, 42.1°W, 6.6 m/pixel). This is one of the highest incidence angle LO images and serves as a good intermediate between the near-terminator image (Fig. 4a) and typical LO images (~70° incidence angle). The third site is a 64 km² area found in the 71° incidence angle image LO3-200-M (~3.1°S, 42.6°W, 6.4 m/pixel) and is representative of typical LO medium resolution images. These sites have estimated ages of 2.08 billion years (+0.65, −0.39) and 2.54 billion years (+0.29, −0.17), respectively (Hiesinger et al. 2003). These are all young mare, and because they are similar in age (the ages of all three sites are within the error bars of each other), they should have similar crater populations.

We digitized craters in each image (over 20,000 craters total) with an interactive monitor-cursor program that fit a circle to three points selected on a crater rim. Craters were

identified as nearly continuous circular features, with the caveat that the extreme shadowing often complicates crater morphology. A simple criterion was used to limit the number of false identifications and maintain consistency from one counting session to the next: if a mental debate occurred as to whether the feature was a crater or not, it was not digitized. The crater count data in Fig. 6 are presented in standard cumulative histogram form (Arvidson et al. 1979). The equilibrium diameter, where the slope of the cumulative histogram begins to deviate from a log-log slope of approximately −3.4 (Soderblom 1970), was found by calculating the slope using points at smaller and smaller crater diameter bins until the slope was less than −3.4. The slopes were found with an iterative least squares fitting routine for non-linear functions originally described by Bevington (1969). In this way, the equilibrium diameter for the 89° incidence image was found to be approximately 260 m, 190 m for the 79° image, and 165 m for the 71° image. We interpret that the incidence angle had a significant effect on the number of craters identified, and thus the equilibrium diameter differed by nearly 100 m for these three areas, even though they are of similar age.

To estimate regolith depth in the 89° image, we compared the percentage of the surface covered by the equilibrium population to the percent of the surface that would be covered by the production population (with a slope of −3.4) (Table 1). We assumed that the equilibrium population actually followed a −2 slope typical of equilibrium populations (Gault 1970; Schultz et al. 1977) in the cumulative histogram, rather than the flat line in Fig. 6a. The very low slope at small diameters is most likely due to small craters being hidden by shadows of larger craters, as well as the resolution limiting the number of craters detected at the smallest sizes. This assumption does not affect our regolith depth estimates significantly because small (compared to the equilibrium diameter) craters do not contribute appreciably to regolith depth, but rather simply rework it (Oberbeck et al. 1973). The difference between the area covered by craters produced on the surface and the area covered by the equilibrium population of craters still present on the surface is the portion of the surface covered by craters that have been obliterated, mainly by infilling of regolith (Shoemaker et al. 1969). Regolith depth in that portion of the surface is equal to the initial average depth of the craters that are now filled in. The maximum crater depth is 20% of crater diameter, including excavation and compression (Pike 1974). The corresponding average crater depth of an idealized bowl-shaped crater with a depth to diameter ratio of 0.2 is 14% of crater diameter. This approximation takes into account the shallowing of the crater near the edges and subtracts the rim height, which does not contribute to the depth of the crater below the preexisting surface.

A key assumption in estimating regolith depth from this method is the initial depth of the craters. While the maximum
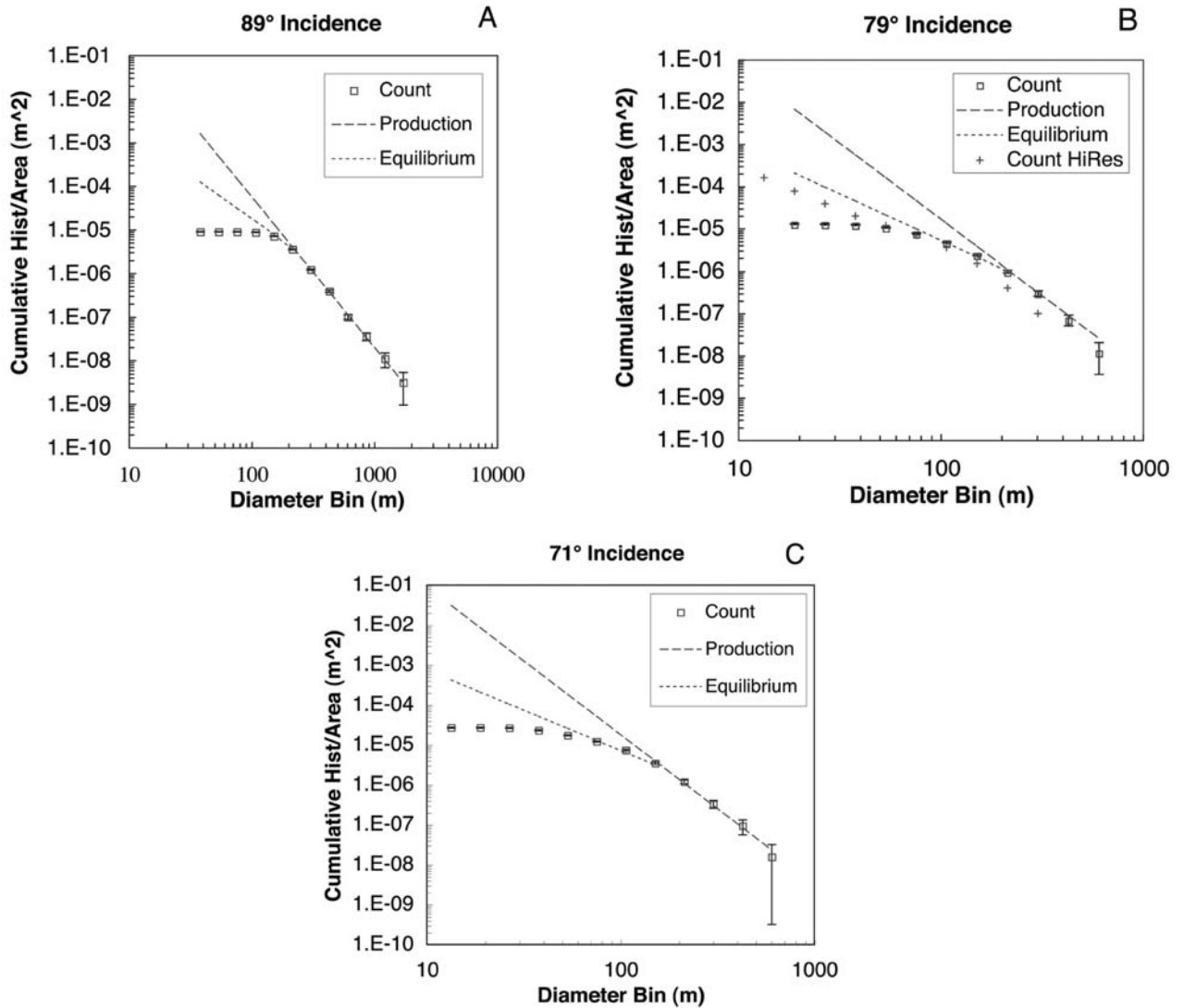
Fig. 6. Cumulative histograms of craters found in our three study areas. The "count" population is the craters counted on the surface, the production population was calculated from the best-fit of craters above the equilibrium diameter, and equilibrium population is assumed to have a –2 log-log slope. a) The 89° incidence angle study area with an equilibrium diameter of ~260 m. b) The 79° incidence angle study area with an equilibrium diameter of ~190 m. Also shown is crater count data from a high-resolution LO image of a portion of the same area. The break in slope is consistent with the medium-resolution data, and shows the equilibrium population of craters. c) The 71° incidence angle study area with an equilibrium diameter of ~165 m. Error bars are 1 σ, as defined by Arvidson et al. (1979).

depth of primary craters is 20% of crater diameter (Pike 1974), it has been suggested that secondary craters are ~50% shallower than primaries (Pike 1980). However, this is for secondary craters that are close to their parent crater, and are clustered so that they often share rims with adjoining secondaries. Secondary craters become better developed with increasing distance from their parent crater, and isolated secondaries far from the parent crater are not significantly affected by debris surges, as is the case with clustered secondaries (Morrison and Oberbeck 1978). Our study areas are relatively far from large secondary-producing impacts. We attempted to avoid areas with obvious secondary craters

using methods described by Neukum et al. (1975) and the criteria of Oberbeck and Morrison (1973) (herringbone pattern, elongated shape, and clustering). To investigate what effects any isolated secondaries remaining in our data set might have, we carried out a cursory examination of the depths of fresh secondary craters of a range of diameters in the image LO3-165-M (outside of our crater count study area) (Fig. 7). Because the incidence angle of this image is 79°, the shadow of any crater with a depth to diameter ratio of 0.2 will fall halfway across the crater floor. Comparing the shadow size to crater size of 50 secondary craters, we find that 90% of the secondary craters have a depth to diameter ratio of ≥0.2.

Table 1. Comparison of production and count populations of crater data from Fig. 5a.

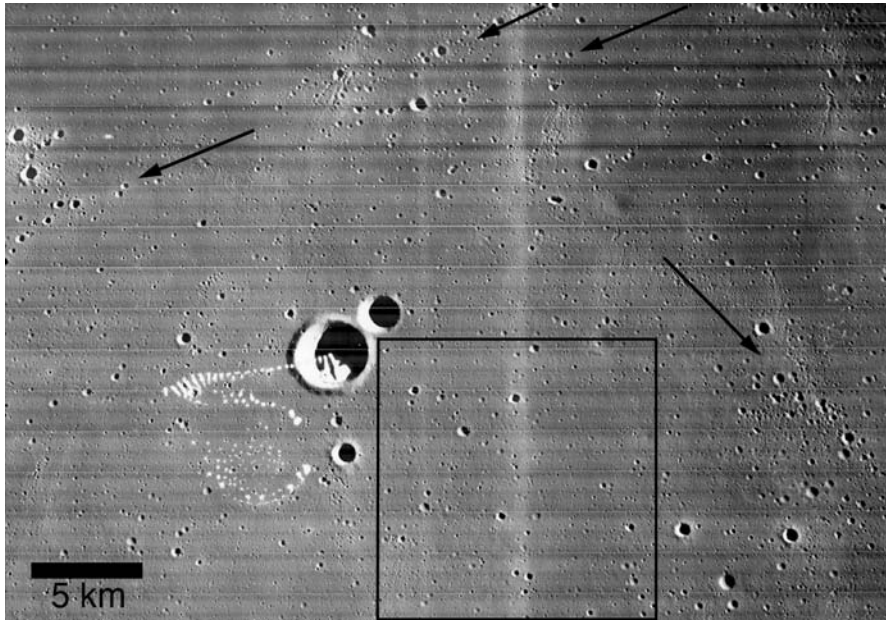| Diameter bin (m)	Equilibrium coverage (%)	Production coverage (%)	Regolith coverage (%)	Maximum depth (m)	Average depth (m)
38	14	182	168	8	5
53	14	110	96	11	8
75	14	67	53	15	11
107	14	40	26	21	15
151	14	24	10	30	22
213	14	15	1	43	31

Fig. 7. A portion of LO3-165-M. The incidence angle of the image is 79°, and thus the shadows of craters with depth to diameter ratios of 0.2 (Pike 1974) should fall halfway across the crater floor; most fresh craters show this relationship. Likely secondary craters are indicated with arrows. The inset box encloses our 79° incidence angle study area, specifically chosen to be away from most of the obvious secondaries. Resolution is 6.6 m/pixel.

Thus, it does not appear that isolated secondaries that might remain in our crater count data were initially significantly shallower or that they would influence our estimates of regolith depth.

Regolith depth estimates were calculated by taking the number of craters lost mainly due to infilling of regolith of each diameter bin and converting that to the percent of the surface that those craters would cover. The regolith depth for that portion of the surface was taken to be 14% of crater diameter, as explained above. This method suggests that for our 89° incidence angle study area, the regolith in nearly the entire area is at least 8 m deep (i.e., the surface is nearly covered with craters 53 m in diameter that have been filled in with regolith). In 53% of the area the regolith is 11 m deep, in 26% of the area the regolith is 15 m deep, in 10% of the area the regolith is 22 m deep, and in 1% of the study area the regolith is 31 m deep. We also examined the sensitivity of the depth estimate to changes in equilibrium diameter, whether due to different lighting conditions as in our three study areas, or because of actual differences in the crater populations. For

a production population with a slope of −3.4, we varied the equilibrium diameter (break point in slope) and calculated the resulting estimated regolith depths (Fig. 8). As the equilibrium diameter increases, the average regolith depth increases and covers a broader range of depths.

Areas of similar age as our study areas have been previously estimated to have a regolith depth of 1–6 m (Oberbeck and Quaide 1968). The median depth (11 m) inferred here is greater than previous estimates and the depth varies significantly (8–31 m) in the region. Our estimate of a deeper regolith is likely due in part to the fact that we found a higher equilibrium diameter than the current paradigm of ~100 m or less for Eratosthenian mare (Wilhelms 1987).

Block Populations

While extremely high incidence angle photography at sufficient resolution is limited to a very few local sites, high resolution images (0.5–2.0 m/pixel) at incidence angles of ~70° exist for a much broader sampling of the lunar surface.

These are the Lunar Orbiter (LO) high-resolution images, and at meter resolution they are well-suited for studying the block populations of craters (Hansen 1970; Anderson and Miller 1971). We investigated craters and their block populations in 23 images (Table 2). Eight of our images are located in western Oceanus Procellarum, two in eastern Oceanus Procellarum, two in Sinus Medii, eight in Mare Tranquillitatis, and three in Mare Fecunditatis. The angular resolution of these images ranges from 65 cm/pixel to 94 cm/pixel, with an average angular resolution of 78 cm/pixel.

A caution for the LO data is that these are digital scans of second or third generation photographic prints, so the effective resolution is estimated to be around a factor of two less than the angular resolution (~2 m/p). This is important for the study of block populations, the identification of which is dependent on the effective resolution. For example, many blocks and crater morphologies that are clearly visible in the LO high resolution set are not detectable or are barely detectable in the LO medium resolution set, at 8 times lower resolution (Fig. 9). To avoid this kind of resolution effect, we have only included craters larger than 50 m in our dataset. The largest blocks associated with craters 50 m in diameter that have not undergone significant degradation typically range in size from 2.9 to 4.4 m (Moore 1971) and are thus large enough to be detected in the LO high resolution images.

We classified all craters (over 800 total) in our images by the density of their block populations (A, B, or C). Craters of class A were distinctly blocky, craters of class B had one to a few blocks, and craters of class C had no blocks. While we made a distinction between craters with abundant blocks and those with just a few blocks, it is not clear that this separation is necessarily significant. A few blocks in a crater could simply represent random "erratics" from nearby crater(s), or could have been buried in the regolith and simply re-excavated by the impact event. However, if even one or two blocks were excavated from the coherent substrate by that cratering event, these blocks are potentially an indicator of regolith depth. In addition, especially for the smaller craters, a crater might have abundant blocks, but only the largest few (>2 m) would be detectable at this resolution. We also noted crater morphology and excluded from our dataset those that were heavily degraded. In these craters, any primary blocks would have a significant chance of being obliterated or buried by the regolith filling the crater.

The craters show a trend of increasing blockiness with increasing diameter (Fig. 10a). If the regolith were of uniform depth, one would expect a single diameter and thus a single depth of excavation greater than which all craters in a given area would be blocky. The regolith depth in this case would be the depth of excavation of this cutoff diameter, where maximum depth of excavation is roughly 10% of the crater diameter (Pike 1974). All craters smaller than this threshold diameter would be excavating only regolith and all craters larger than the threshold would excavate the coherent
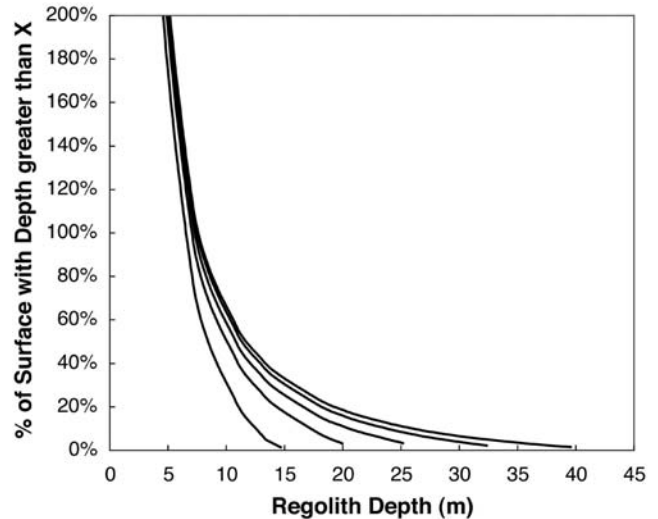

Fig. 8. Regolith depth versus equilibrium diameter; curves represent increasing equilibrium diameter. From left to right: 100 m, 150 m, 200 m, 250 m, and 300 m, respectively. The depths were calculated by varying the equilibrium diameter, assuming a production slope of −3.4 and an equilibrium slope of −2. Average regolith depth and the range of depths increase with equilibrium diameter.

substrate to some extent. This simple model is not the case. Instead, the data show a more gradual trend, where only ~10% of craters in the 75 m bin are excavating blocks, with this number increasing with diameter until all craters >525 m are excavating blocks. As discussed below, this observation is consistent with a regolith that is not all one depth, but has considerable lateral variability and does not have a strict boundary between coherent and incoherent material.

Maria of different ages show distinct block population trends (Figs. 10b and 10c). The portion of our study area located in Oceanus Procellarum near the Surveyor I landing site is the youngest, with an estimated age of ~2.5 billion years (Boyce 1976; Whitford-Stark and Head 1980; Hiesinger et al. 2003). The oldest portion of our study area is ~3.6 billion years in Mare Tranquillitatis (Boyce 1976; Hiesinger et al. 2000). For the oldest surface, 10% of the craters 75 m in diameter are blocky and all craters >475 m are blocky. Thus, in this older area, 90% of the regolith is >8 m deep and all of the regolith is <48 m deep. This estimate is deeper than previous estimates of 3–5 m for Mare Tranquillitatis at the Surveyor V site (Shoemaker and Morris 1969) and a range of 1–10 m for three selected sites in Mare Tranquillitatis (Oberbeck and Quaide 1968). As expected, the younger surface (Oceanus Procellarum) has a distinctly blockier surface. At 75 m in diameter, 10% of all craters are blocky. Above 325 m all craters are blocky. Thus, 90% of the regolith is >8 m deep and the regolith everywhere is <33 m deep in the younger area. However, these depths are necessarily approximate because of possible origins for the blocks other than from coherent bedrock. As noted above,

Table 2. Lunar Orbiter images used in the study of block populations.

Image	Area (km^2)	Latitude	Longitude	Resolution (m/p)	Location[a]
LO3-205-H2	14.05	−2.16	−44.79	0.9	PR-W
LO 3-188-H2	17.82	−2.46	−44.25	0.8	PR-W
LO 3-191-H3	9.99	−2.62	−43.83	0.8	PR-W
LO 3-181-H2	9.92	−2.22	−43.50	0.8	PR-W
LO 3-195-H2	10.04	−2.83	−43.26	0.8	PR-W
LO 3-184-H2	27.38	−2.38	−43.07	0.8	PR-W
LO 3-200-H2	10.10	−3.10	−42.56	0.8	PR-W
LO 3-167-H2	10.47	1.55	−41.83	0.8	PR-W
LO 3-153-H2	8.23	−2.97	−23.51	0.7	PR-E
LO 3-148-H1	8.10	−2.85	−22.74	0.7	PR-E
LO 3-94-H1	6.77	0.92	−1.63	0.7	SM
LO 3-99-H2	6.54	0.69	−1.03	0.7	SM
LO 2-69-H3	6.80	2.70	24.62	0.7	TR
LO 2-83-H3	8.26	1.00	24.66	0.7	TR
LO 2-70-H1	6.80	2.67	24.75	0.7	TR
LO 2-73-H1	6.84	2.60	25.11	0.7	TR
LO 3-12-H1	10.90	2.71	32.25	0.8	TR
LO 3-10-H1	11.26	2.82	34.95	0.8	TR
LO 3-16-H2	10.82	2.49	35.82	0.8	TR
LO 3-20-H1	10.43	2.27	36.39	0.8	TR
LO 3-26-H1	10.04	−0.85	42.12	0.8	MF
LO 3-35-H3	12.03	−1.05	42.81	0.9	MF
LO 3-32-H1	10.13	−1.16	42.93	0.8	MF
	Total area: 243.71			Average resolution: 0.8	

[a]PR-W = Oceanus Procellarum West, PR-E = Oceanus Procellarum East, SM = Sinus Medii, TR = Mare Tranquillitatis, MF = Mare Fecunditatis.
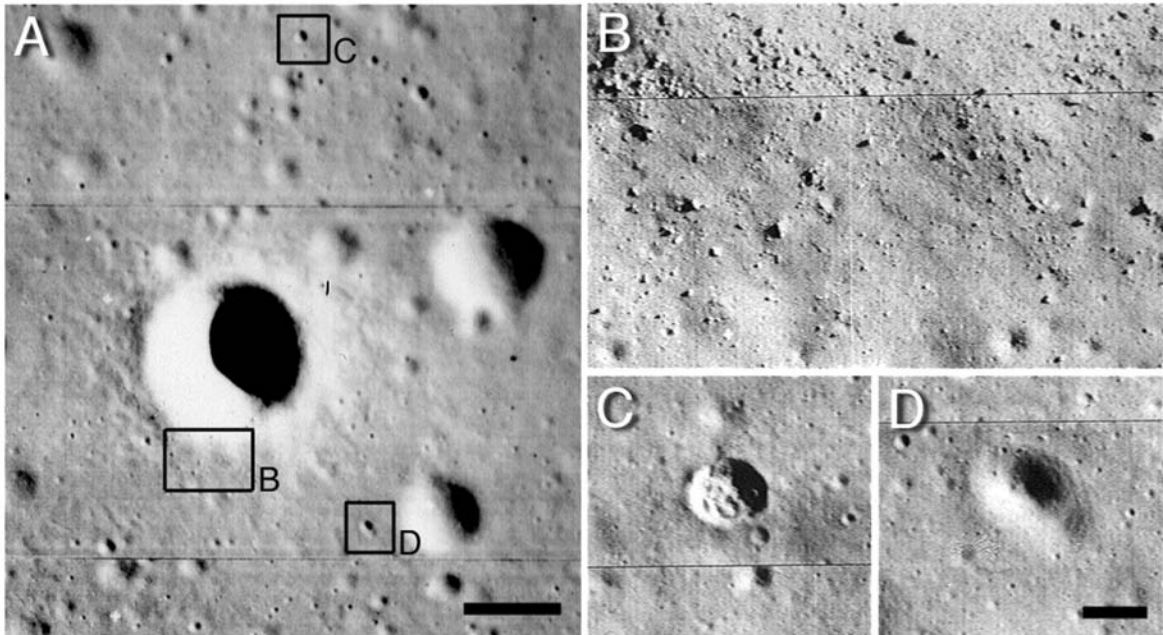

Fig. 9. a) A medium-resolution LO image that shows the locations of the high-resolution LO images (b–d). b) Blocky ejecta blanket; only the largest blocks are also detectable in (a). c) A crater with irregular morphology indicative of more coherent substrate. d) A crater with normal, bowl-shaped morphology. Note that the different morphologies of (c) and (d) are indistinguishable in the LO medium-resolution image. The scale bar for (a) is 500 m; the scale bar for b–d is 50 m. LO3-185-M (6.4 m/pixel), LO3-205-H (0.9 m/pixel).

some could have been buried blocks that were simply re-excavated from the regolith or blocks that were produced from induration of the regolith. Both of these cases would lead to underestimation of the actual regolith depth.

The young Procellarum surface (2.54 billion years) is estimated to be similar in age to our 89° incidence angle study area (2.76 billion years) (Hiesinger et al. 2003), and the results for regolith depth using these two different methods (block population and equilibrium diameter) compare favorably. From both methods, the regolith in each of the younger areas is estimated to be ~8–32 m deep, compared to previous estimates of 1–3 m at the Surveyor I site (Shoemaker and Morris 1969) and a range of 1–6 m for this same site (Oberbeck and Quaide 1968). Oberbeck and Quaide (1968) also find a median thickness of 3.3 m for this site, compared to our median thickness of 11 m.

In the younger Procellarum area (thinner regolith) there are 5.0 small (50–250 m in diameter) craters per km^2 (109.8 km^2 sample area), while in the older Tranquillitatis area (thicker regolith) there are 2.2 small craters per km^2 (72.1 km^2 sample area). Thus, in the younger mare there are 2.3 times as many small craters per unit area than in the older mare, a seemingly counterintuitive result. The difference in the populations of craters in the diameter range of 50 to 250 m is most likely due to the more efficient degradation of small craters in areas of deeper regolith (older mare). Because they penetrate only to a shallow depth, small craters form mostly in loose regolith instead of coherent bedrock and thus are more easily degraded per unit of time in the older mare (Trask and Rowan 1967; Lucchitta and Sanchez 1975; Robinson et al. 2002; Wilcox et al. 2002). A similar phenomenon occurs in the highlands, where there are fewer small craters per unit area than in the mare, despite the older age of the highlands. This difference is attributed to the thicker regolith in the highlands and thus more efficient degradation of craters that form mainly in regolith (Robinson et al. 2002).

Small Crater Optical Maturity

Clementine multi-spectral images provide a further constraint on regolith depth. Optical maturity (OMAT) parameter images (Lucey et al. 2000) show the relative maturity or "freshness" of a material exposed on the lunar surface. OMAT values are based on the relative positions on a plot of the ratio of 950/750 nm reflectances versus 750 nm reflectance. The further the radial distance from a hypothetical fully mature end member, the higher the OMAT value and the higher degree of immaturity (Lucey et al. 2000). Thoroughly gardened regolith that has been exposed for a long period of time will have low OMAT values; more recently exposed regolith or rock will have higher OMAT values (Lucey et al. 2000). The utility of OMAT in terms of estimating regolith depth lies in the fact that the amount of fresh material excavated by a crater will depend on the ratio of
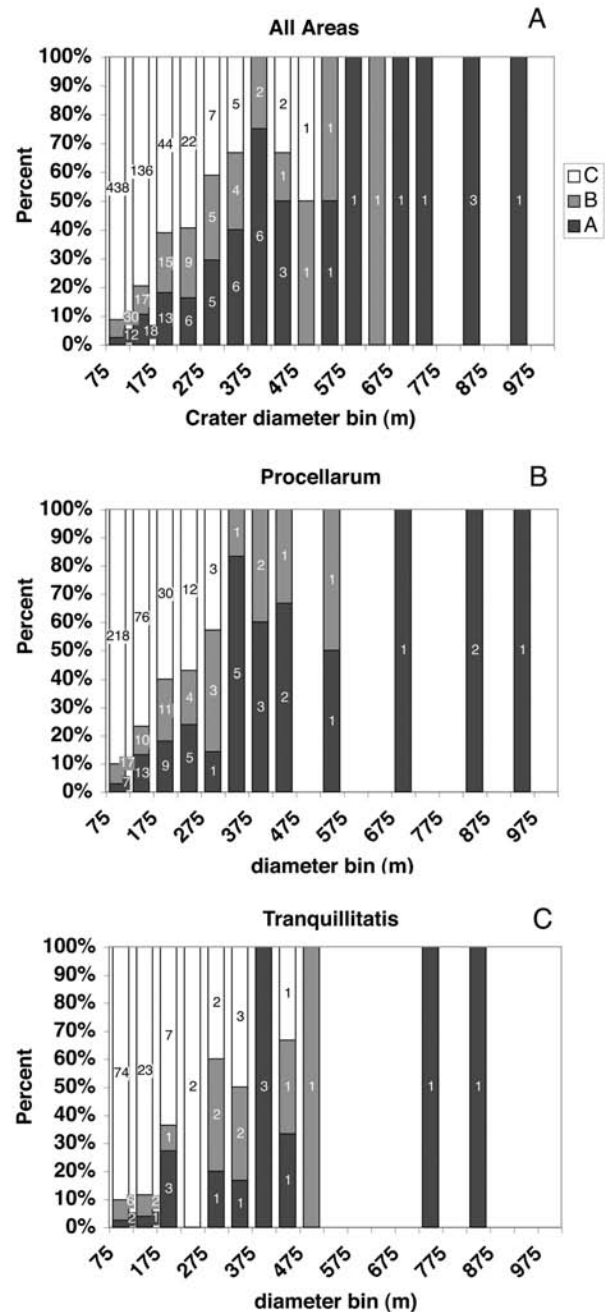

Fig. 10. a) The distribution of blocky craters classes A–C by diameter in our study areas. b) The percent of blocky craters versus diameter in western Procellarum, the youngest portion of our study area. c) The percent of blocky craters versus diameter in Tranquillitatis, the oldest portion of our study area. Craters with the most degraded morphology have been excluded. Numbers overlying graph are the number of craters in each bin.

the crater's depth to the depth of the regolith. In a thick regolith, a large portion of the material excavated by small craters will be material that has reached varying degrees of optical maturity. In areas of thinner regolith, small craters will penetrate through the mature regolith and excavate a larger
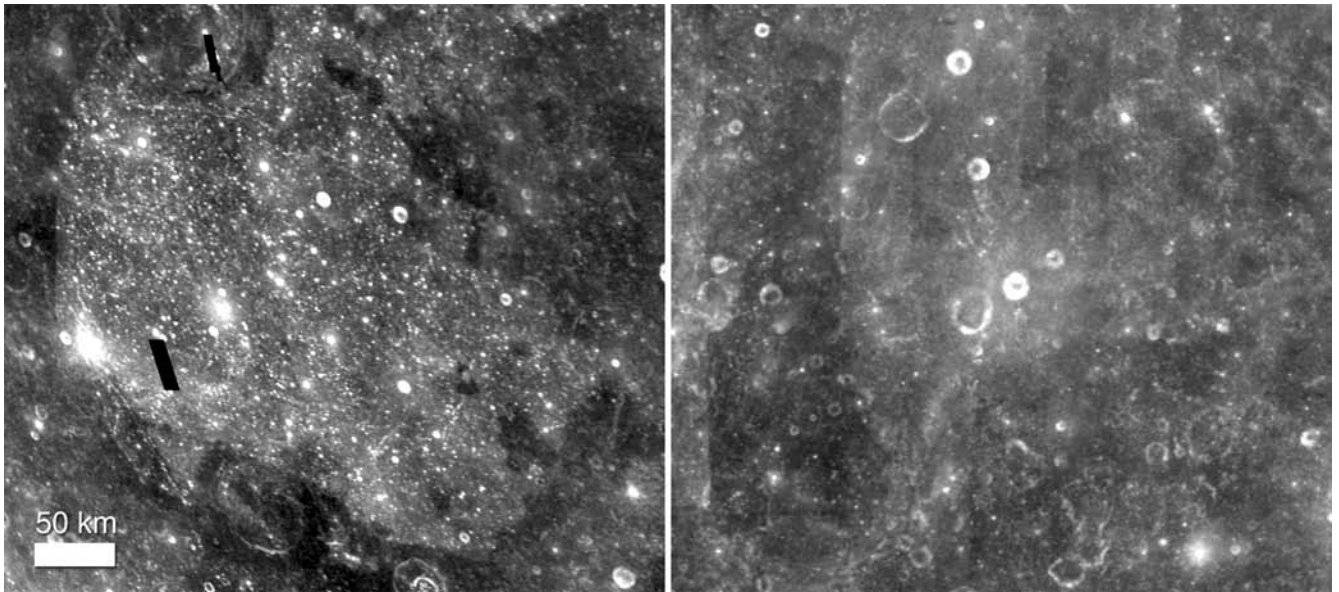
Fig. 11. OMAT images (brighter or higher values indicate immature material, while darker or lower values indicate mature material) of Mare Humorum on the left (centered at −23.39, −37.18) and a highlands area on the right (centered at −9.52, 5.34). In the image on the left, the greater number of small, immature craters in Mare Humorum can be seen (0.47% of image has OMAT > 0.3), and the mare/highlands border is visible as a sharp drop-off in the number of small, immature craters. In the image on the right, the highlands show relatively few small, immature craters (0.04% of image has OMAT > 0.3). Scale bar applies to both images.

Table 3. Abundance of small (<500 m), immature craters in selected mare and highlands sites.

Region	Number of small, immature craters	Study area (km^2)	Small, immature craters/km^2
Oceanus Procellarum	1229	142,100	8.6×10^{-3}
Mare Serenitatis	764	101,300	7.5×10^{-3}
Mare Frigoris	156	35,500	4.4×10^{-3}
Lacus Somniorum	53	33,100	1.6×10^{-3}
Mare Nectaris	44	73,300	6.0×10^{-4}
Apollo 16 highlands	22	38,273	5.7×10^{-4}
Apollo 14 highlands	6	23,726	2.5×10^{-4}
Mare Tranquillitatis	28	299,000	9.4×10^{-5}

portion of fresh material that will be detectable in the OMAT image. This method is similar in principle to the blocky crater method, with fresh material analogous to blocks as indicators of penetration through the regolith.

For determination of absolute regolith depths in an area, the resolution of Clementine images is prohibitively low (100 m/pixel). To determine absolute depths, it would be necessary to be able to measure craters as small as 10 m that excavate to a depth of as little as 1 m. However, a comparison of the relative number of small optically immature craters between different mare and highland units could potentially indicate relative regolith depths. Areas of shallow regolith would have the most small, immature craters; areas of deep regolith would have the fewest small immature craters, as small craters would be less likely to excavate optically immature material (Fig. 11). To test this hypothesis, we selected all of the fresh craters smaller than 500 m in eight mare and highlands regions (Table 3). A cutoff value of

OMAT >0.3 was chosen because this represents the least mature material, 2.3% of the lunar surface (Lucey 2004). An absolute determination of crater diameter is hindered by the fact that the craters of interest are near the resolution limit of the images and because their bright ejecta blankets mask the boundary of the crater rim. Thus, we can only bracket their diameters as between 100–500 m.

The abundance of the small, immature craters per unit area would suggest the increasing order of regolith depths as listed in Table 3. This order is consistent with the order of ages of the regions, with the exception of Mare Tranquillitatis (Wilhelms 1987). The high opaque mineral content of Mare Tranquillitatis could be affecting the OMAT parameter in this region, as noted by Lucey et al. (2000), thus affecting the number of craters that are identified as immature. The OMAT method is promising and could become a powerful regolith depth indicator with the eventual acquisition of high-resolution (10 m/pixel or better) multispectral data.
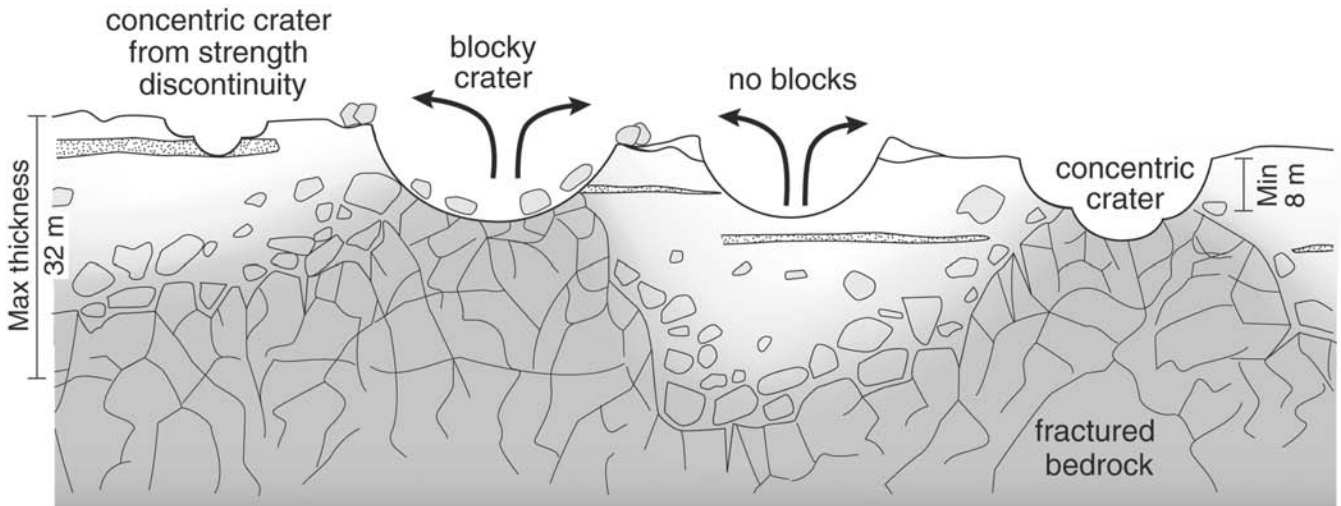
Fig. 12. A model of the lunar regolith showing the uneven, irregular, and fractured bedrock surface that grades upward into less cohesive material. Craters with blocks were formed during impact into bedrock, craters without blocks formed only in regolith. Concentric craters are shown both as the result of impact into a strength discontinuity such as an ejecta blanket, and impact into bedrock. Regolith depth can vary by approximately a factor of five within a small area (hundreds of meters). In the highlands, the substrate is most likely composed of hundreds of meters to kilometers of basin ejecta (megaregolith), while in the mare the substrate consists of layered basaltic material, possibly with intercalated ejecta and regolith layers.

DISCUSSION

A key finding of this work is that the equilibrium diameter predicted from crater counts is sensitive to the solar incidence angle of the image(s) used for crater counting as first proposed by Young (1975). In our three study areas, we found that as incidence angle increases from 71° to 79° to 89°, the estimate of equilibrium diameter grows from 165 m to 190 m to 260 m due to an increase in the number of craters that are visible. The equilibrium diameter in turn has significant implications for inferred regolith depth (Fig. 8). For example, a change from an equilibrium diameter of 100 m to 150 m translates to a 25% increase in the median regolith depth; the difference between a 100 m and 250 m equilibrium diameter results in a 50% increase in the median depth estimate. The range of regolith depths also increases with equilibrium diameter: the minimum depth estimate changes little, while the maximum increases significantly. At 100 m equilibrium diameter, the estimated regolith depth ranges from ~7 to 15 m. At 300 m equilibrium diameter, the inferred depth ranges from ~8 to 40 m. Accurate determination of the equilibrium diameter is thus critical for determining regolith depth.

Usually it is difficult to determine unambiguously the diameter at which the transition to equilibrium cratering occurs. Instead of a sharp break in slope, from −3.4 to −2.0 on a cumulative plot, there is often more of a gradual rolling over. Cumulative histogram slopes and breakpoints might be enhanced and the equilibrium diameter might become more readily apparent if larger areas were included in the crater counts. In some cases this is not possible, as in the 89° incidence angle image, where there is only limited

photographic coverage. Though near terminator images clearly allow the detection of more craters on the surface than do images at 70° incidence, they are still not ideal. The shadows of even small topographic features become so pronounced that they often hide any nearby smaller features. This effect results in the smaller craters often being hidden in the shadows of larger ones, and in cumulative histograms this is seen as a flattening of the slope to nearly zero at small diameters (Soderblom 1972).

A further test of the effects of incidence angle with existing data would be to compare the Apollo pan images at their full resolution (~2 m/pixel at the center of the image, degrading radially outward) to LO images (Masursky et al. 1978). The pan images exist at a wider variety of incidence angles because they were taken in an equatorial orbit from terminator to terminator, and have overlapping coverage at a different incidence angle from the LO images, which are nearly all ~70° incidence because they were taken in polar orbit. Laser altimetry or stereo image-based digital elevation models from future missions at 5 m/pixel or better would allow unambiguous crater counts down a diameter of ~25 m, thus allowing confident identification of slope breakpoints in the crater size-frequency distributions and equilibrium sizes. Such data at 5 m/pixel might be more accurate than imaging at 1 m/pixel because of the ability to produce shaded relief images at any desired incidence angle.

Identifying the distribution of blocky craters over a large area provides an independent test to the equilibrium diameter method for determining regolith depth. Previously, this method was applied in the immediate vicinity of Surveyor landers where only a limited number of craters of the desired size range were observable (Shoemaker and Morris 1969).

Since the craters observed in the Surveyor images are only representative of the depth at one small spot (tens of meters in diameter), they probably do not represent regolith depths over a broader area (i.e., the whole geologic unit sampled by a particular Surveyor spacecraft). In our study, we have observed a wide range of crater sizes over a much larger area, and find a range in regolith depth predicted by block populations that is in agreement with the range obtained from the equilibrium diameter method.

Studying the number of small optically immature craters has the potential to give relative regolith depths (Table 3), though areas with high opaque content, like Mare Tranquillitatis, are an exception and a correction for composition would have to be developed. This method has the potential to give absolute depths through the study of the size-frequency distribution of small fresh craters, but much higher resolution images (1–10 m/pixel) would be required to measure and count craters as small as 10–50 m in diameter.

A close examination of the various definitions of regolith has been given in order to determine whether there are differences in regolith depth estimates simply because of differences in the definition of regolith itself. The difference between our regolith depth estimates and previous estimates is not just a question of definition. Quaide and Oberbeck (1968), using the most inclusive definition of regolith, still find a shallower regolith depth (1–6 m) for Eratosthenian mare surfaces similar to those that we investigated. We suggest the difference is due to the fact that their crater morphology method is not necessarily always indicating the regolith-bedrock transition, but perhaps a transition of grain sizes, buried ejecta layers, or any kind of strength discontinuity. A key question that remains is what percentage of the bench or concentric craters are actually due to the regolith-bedrock interface, and what percent are due to factors such as those listed above.

Using two independent methods, we estimate that the regolith depth in three Eratosthenian (2.0 to 2.5 billion years) mare areas ranges from approximately 8 to 32 m locally (median depth of 11 m). The significance of the variability of the regolith depth within a local area (same unit) is not always appreciated, and this is reflected in the flat, simple regolith structure paradigm that often prevails-a tabular layer of loose regolith atop a planar bedrock surface (see, e.g., Fig. 15 of Cooper et al. 1974; Figs. 10.23, 11.12, and 12.15 of Wilhelms 1987; Fig. 10.19 of Heiken et al. 1991). Such a model is not supported by our data or previous work. A more representative model of the regolith has an uneven, undulating and fractured bedrock surface that grades upward into less and less cohesive material (Fig. 12).

Knowledge of regolith depths is important for the interpretation of remote sensing data and the planning of sample retrieval on the Moon and on other bodies. Regolith excavated from different depths transfers materials to the surface from different portions of a layered target, mixing spectral signatures for remote sensing and also determining what is easily obtained for samples. Interpretation of the results from the upcoming Dawn mission to explore the asteroids Ceres and Vesta (Russell et al. 2003) will depend on understanding the regolith, where questions of exposure of varied differentiation products and surface modification will be affected by the amount and distribution of regolith. Interpretive problems from varied and gradational regolith properties on asteroid Eros have been noted by various authors (Thomas et al. 2001; Robinson et al. 2002; Chapman et al. 2002).

Understanding the regolith will also be important in the upcoming MESSENGER mission, which will map the surface of Mercury in the UV-VIS-NIR to a scale of ~200 m/pixel and locally return much higher resolution (10 m/pixel) BW images. One of the key science goals is unraveling the evolution of the mercurian crust through superposition and color/mineralogic interpretations (Solomon et al. 2001). These interpretations may critically depend on an awareness of mixing processes caused by regolith development in a layered target (i.e., volcanic flows) with thicknesses at the scale of significant regolith overturn. Previous studies of the lunar regolith as well as the results presented here emphasize the need for a thorough understanding of the depth of a regolith to maximize the science return from remote sensing, as well as landed science and returned samples.

Editorial Handling—Dr. Beth Ellen Clark

REFERENCES

Anderson A. T. and Miller E. R. 1971. Lunar Orbiter photographic supporting data. NASA National Space Science Data Center Publication 71–13. 511 p.

Arvidson R. E., Boyce J., Chapman C., Cintala M., Fulchignoni M., Moore H., Neukum G., Schultz P., Soderblom L., Strom R., Woronow A., and Young R. 1979. Standard techniques for presentation and analysis of crater size-frequency data. *Icarus* 37:467–474.

Arvidson R. E., Drozd R. J., Hohoenberg C. M., Morgan C. J., and Poupeau G. 1975. Horizontal transport of the regolith, modification of features, and erosion rates on the lunar surface. *The Moon* 13:67–79.

Bevington P. 1969. *Data reduction and error analysis for the physical sciences*. New York: McGraw-Hill. pp. 237–239.

Boyce J. M. 1976. Ages of flow units in the lunar nearside maria

based on Lunar Orbiter IV photographs. Proceedings, 7th Lunar Science Conference. pp. 2717–2728.

Chapman C. R., Merline W. J., Thomas P. C., Joseph J., Cheng A. F., and Izenberg N. 2002. Impact history of Eros: Craters and boulders. *Icarus* 155:104–118.

Cintala M. J. and McBride K. M. 1995. Block distribution on the lunar surface: A comparison between measurements obtained from surface and orbital photography. NASA Technical Memorandum #104804. Houston: NASA Johnson Space Center. 41 p.

Cooper M. R., Kovach R. L., and Watkins J. S. 1974. Lunar near-surface structure. *Reviews of Geophysics and Space Physics* 12: 291–308.

Crozaz G., Walker R., and Woolum D. 1971. Nuclear track studies of dynamic surface processes on the Moon and the constancy of solar activity. Proceedings, 2nd Lunar Science Conference. pp. 2543–2558.

Gault D. E. 1970. Saturation and equilibrium conditions for impact cratering on the lunar surface: Criteria and implications. *Radio Science* 5:273–291.

Gault D. E., Hörz F., and Hartung J. B. 1972. Effects of microcratering on the lunar surface. Proceedings, 3rd Lunar Science Conference. pp. 2713–2734.

Hansen T. P. 1970. Guide to Lunar Orbiter photographs. NASA Special Paper #242. Washington, D.C.: U.S. Government Printing Office. 125 p.

Heiken G. H., Vaniman D. T., and French B. M. 1991. *Lunar sourcebook: A user's guide to the Moon*. Cambridge: Cambridge University Press. 736 p.

Hiesinger H., Jaumann R., Neukum G., and Head J. W. III. 2000. Ages of mare basalts on the lunar nearside. *Journal of Geophysical Research* 105:29,239–29,275.

Hiesinger H., Head J. W., III, Wolf U., Jaumann R., and Neukum G. 2003. Ages and stratigraphy of mare basalts in Oceanus Procellarum, Mare Nubium, Mare Cognitum, and Mare Insularum. *Journal of Geophysical Research* 108, doi:10.1029/2002JE001985.

Hörz F. 1977. Impact cratering and regolith dynamics. *Physics and Chemistry of the Earth* 10:3–15.

Hörz F., Schneider E., and Hill R. 1974. Micrometeoroid abrasion of lunar rocks: A Monte Carlo simulation. Proceedings, 5th Lunar Science Conference. *Geochimica et Cosmochimica Acta,* Supplement 5:2397–2412.

Latham G. V., Ewing M., Press F., Sutton G., Dorman J., Nakamura Y., Toksöz N., Wiggins R., and Kovach R. 1970. Passive seismic experiment. In Apollo 12 preliminary science report. NASA Special Paper #235. Washington, D.C.: U.S. Government Printing Office. pp. 39–54.

Latham G. V., Ewing M., Press F., Sutton G., Dorman J., Nakamura Y., Toksöz N., Duennebier F., and Lammlein D. 1971. Passive seismic experiment. In Apollo 14 preliminary science report. NASA Special Paper #272. Washington, D.C.: U.S. Government Printing Office. pp. 133–162.

Latham G. V., Ewing M., Press F., Sutton G., Dorman J., Nakamura Y., Toksöz N., Lammlein D., and Duennebier F. 1972. Passive seismic experiment. In Apollo 15 preliminary science report. NASA Special Paper #289. Washington, D.C.: U.S. Government Printing Office. pp. 8-1–8-25.

Lucchitta B. K. and Sanchez A. G. 1975. Crater studies in the Apollo 17 region. Proceedings, 6th Lunar and Planetary Science Conference. pp. 2427–2441.

Lucey P. G. 2004. Mineral maps of the Moon. *Geophysical Research Letters* 31, doi:10.1029/2003GL019406.

Lucey P. G., Blewett D. T., Taylor G. J., and Hawke B. R. 2000. Imaging of lunar surface maturity. *Journal of Geophysical Research* 105:20,377–20,386.

Masursky H., Colton G. W., and El-Baz F. 1978. Apollo over the Moon. NASA Special Paper #362. Washington, D.C.: U.S. Government Printing Office. 255 p.

Melosh H. J. 1989. *Impact cratering: A geologic process*. New York: Oxford University Press. 245 p.

Merrill G. P. 1897. *Rocks, rock-weathering and soils*. New York: MacMillan Company. 411 p.

Moore H. J. 1971. Large blocks around lunar craters. In Analysis of Apollo 10 photography and visual observations. NASA Special Paper #232. Washington, D.C.: U.S. Government Printing Office. pp. 26–27.

Morrison R. H. and Oberbeck V. R. 1978. A comparison and thickness model for lunar impact crater and basin deposits. Proceedings, 9th Lunar and Planetary Science Conference. pp. 3763–3785.

Muehlberger W. R., Batson R. M., Boudette E. L., Duke C. M., Eggleton R. E., Elston D. P., England A. W., Freeman V. L., Hait M. H., Hall T. A., Head J. W., Hodges C. A., Holt H. E., Jackson E. D., Jordan J. A., Larson K. B., Milton D. J., Reed V. S., Rennilson J. J., Schaber G. G., Schafer J. P., Silver L. T., Stuart-Alexander D., Sutton R. L., Swann G. A., Tyner R. L., Ulrich G. E., Wilshire H. G., Wolfe E. W., and Young J. W. 1972. Preliminary investigation of the Apollo 16 landing site. In Apollo 16 Preliminary science report. NASA Special Paper #315. Washington, D.C.: U.S. Government Printing Office. pp. 6-1–6-81.

Muehlberger W. R., Batson R. M., Cernan E. A., Freeman V. L., Hait M. H., Holt H. E., Howard K. A., Jackson E. D., Larson K. B., Reed V. S., Rennilson J. J., Schmitt H. H., Scott D. H., Sutton R. L., Stuart-Alexander D., Swann G. A., Trask N. J., Ulrich G. E., Wilshire H. G., and Wolfe E. W. 1973. Preliminary geologic investigation of the Apollo 17 landing site. In Apollo 17 preliminary science report. NASA Special Paper #330. Washington, D.C.: U.S. Government Printing Office. pp. 6-1–6-71.

Neukum G., Koenig B., and Arkani-Hamed J. 1975. A study of lunar impact crater-size distributions. *The Moon* 12:201–229.

Oberbeck V. R. and Morrison R. H. 1973. On the formation of the lunar herringbone pattern. Proceedings, 4th Lunar Science Conference. *Geochimica et Cosmochimica Acta,* Supplement 4: 107–123.

Oberbeck V. R. and Quaide W. L. 1968. Genetic implications of lunar regolith thickness variations. *Icarus* 9:446–465.

Oberbeck V. R., Quaide W. L., Mahan M., and Paulson J. 1973. Monte Carlo calculations of lunar regolith thickness distributions. *Icarus* 19:87–107.

Pike R. J. 1974. Depth/diameter relations of fresh lunar craters: Revision from spacecraft data. *Geophysical Research Letters* 1: 291–294.

Pike R. J. 1980. Geometric interpretation of lunar craters. Apollo 15–17 orbital investigations. U.S. Geological Survey Professional Paper #1046-C. Washington, D.C.: U.S. Government Printing Office.

Quaide W. L. and Oberbeck V. R. 1968. Thickness determinations of the lunar surface layer from lunar impact craters. *Journal of Geophysical Research* 73:5247–5270.

Rennilson J. J., Dragg J. L., Morris E. C., Shoemaker E. M., and Turkevich A. 1966. Lunar surface topography. In Surveyor I mission report, part II: Scientific data and results. NASA JPL Technical Report #32-1023. pp. 7–44.

Robinson M. S., Thomas P. C., Veverka J., Murchie S. L., and Wilcox B. B. 2002. The geology of 433 Eros. *Meteoritics & Planetary Science* 37:1651–1684.

Russell C. T., Coradini A., De Sanctis M. C., Feldman W. C., Jaumann R., Konopliv A. S., McCord T. B., McFadden L. A., McSween H. Y., Mottola S., Neukum G., Pieters C. M.,

Prettyman T. H., Raymond C. A., Smith D. E., Sykes M. V., Williams B. G., Wise J., and Zuber M. T. 2003. Dawn mission: A journey in space and time (abstract #1473). 34th Lunar and Planetary Science Conference. CD-ROM.

Schultz P. H., Greeley R., and Gault D. 1977. Interpreting statistics of small lunar craters. Proceedings, 8th Lunar and Planetary Science Conference. pp. 3539–3564.

Schmitt H. H. 1973. Apollo 17 report on the Valley of Taurus-Littrow. *Science* 182:681–690.

Shoemaker E. M. and Morris E. C. 1969. Thickness of the regolith. In Surveyor: Program results. NASA Special Paper #184. Washington, D.C.: U.S. Government Printing Office. pp. 96–98.

Shoemaker E. M., Batson R. M., Holt H. E., Morris E. C., Rennilson J. J., and Whitaker E. A. 1967. Television observations from Surveyor III. In Surveyor III mission report, part II: Scientific results. NASA JPL Technical Report #32-1177. pp. 9–67.

Shoemaker E. M., Batson R. M., Holt H. E., Morris E. C., Rennilson J. J., and Whitaker E. A. 1968. Television observations from Surveyor VII. In Surveyor VII: A preliminary report. NASA Special Paper #173. Washington, D.C.: U.S. Government Printing Office. pp. 13–81.

Shoemaker E. M., Batson R. M., Holt H. E., Morris E. C., Rennilson J. J., and Whitaker E. A. 1969. Observations of the lunar regolith and the Earth from the television camera on Surveyor 7. *Journal of Geophysical Research* 74:6081–6119.

Shoemaker E. M., Batson R. M., Bean A. L., Conrad C., Jr., Dahlem D. H., Goddard E. N., Hait M. H., Larson K. B., Schaber G. G., Schleicher D. L., Sutton R. L., Swann G. A., and Waters A. C. 1970. Preliminary geologic investigation of the Apollo 12 landing site, part A. In Apollo 12 preliminary science report, NASA Special Paper #235. Washington, D.C.: U.S. Government Printing Office. pp. 113–156.

Soderblom L. A. 1970. A model for small-impact erosion applied to the lunar surface. *Journal of Geophysical Research* 75:2655–2661.

Soderblom L. A. 1972. The process of crater removal in the lunar maria. In Apollo 15 preliminary science report. NASA Special Paper #289. Washington, D.C.: U.S. Government Printing Office. pp. 25-87–25-91.

Solomon S. C., McNutt R. L., Jr., Gold R. E., Acuña M. H., Baker D. N., Boynton W. V., Chapman C. R., Cheng A. F., Gloeckler G., Head J. W., III, Krimigis S. M., McClintock W. E., Murchie S. L., Peale S. J., Phillips R. J., Robinson M. S., Slavin J. A., Smith D. E., Strom R. G., Trombka J. I., and Zuber M. T. 2001. The MESSENGER mission to Mercury: Scientific objectives and implementation. *Planetary and Space Science* 49:1445–1465.

Swann G. A., Bailey N. G., Batson R. M., Freeman V. L., Hait M. H., Head J. W., Holt H. E., Howard K. A., Irwin J. B., Larson K. B., Muehlberger W. R., Reed V. S., Rennilson J. J., Schaber G. G., Scott D. R., Silver L. T., Sutton R. L., Ulrich G. E., Wilshire H. G., and Wolfe E. W. 1972. Preliminary investigation of the Apollo 15 landing site. In Apollo 15 preliminary science report. NASA Special Paper #289. Washington, D.C.: U.S. Government Printing Office. pp. 5-1–5-112.

Thomas P. C., Veverka J., Robinson M. S., and Murchie S. 2001. Shoemaker crater as the source of most ejecta blocks on the asteroid 433 Eros. *Nature* 413:394–396.

Trask N. J. and Rowan L.C. 1967. Lunar Orbiter photographs: Some fundamental observations. *Science* 158:1529–1535.

Watkins J. S. and Kovach R. L. 1973. Seismic investigation of the lunar regolith. Proceedings, 4th Lunar Science Conference. *Geochimica et Cosmochimica Acta,* Supplement 4:2561–2574.

Whitford-Stark J. L. and Head J. W. 1980. Stratigraphy of Oceanus Procellarum basalts: Sources and styles of emplacement. *Journal of Geophysical Research* 85:6579–6609.

Wilcox B. B., Robinson M. S., and Thomas P. C. 2002. Regolith thickness, distribution and processes examined at sub-meter resolution (abstract #3048). Workshop on the Moon Beyond 2002. CD-ROM.

Wilhelms D. E. 1987. The geologic history of the Moon. USGS Professional Paper #1348. Washington, D.C.: U.S. Government Printing Office. 302 p.

Young R. A. 1975. Mare crater size-frequency distributions: implications for relative surface ages and regolith development. Proceedings, 6th Lunar Science Conference. *Geochimica et Cosmochimica Acta,* Supplement 6:2645–2662.